NANO LETTERS

2007
Vol. 7, No. 6
1449−1453

# Near-Field Evidence for Ferromagnetic "Nanoneedles" in $Nd_{1/2}Sr_{1/2}MnO_3$

**Paul W. Kolb,*,† Danilo B. Romero,† H. Dennis Drew,† Andrei B. Sushkov,‡ Satish B. Ogale,§ and Yutaka Moritomo⊥**

*Laboratory for Physical Sciences, University of Maryland, College Park, Maryland 20740*

*Received December 18, 2006; Revised Manuscript Received March 27, 2007*

**ABSTRACT**

**We report on the near-field optical microscopic (NSOM) imaging of single-crystal $Nd_{1/2}Sr_{1/2}MnO_3$ near the first-order phase transition from the CE-type charge-ordered insulator (COI) to the ferromagnetic metal (FMM) at 165 K. Using polarized light, the measurements are sensitive to twin domains through optical anisotropy and to hysteretic inhomogeneous strain associated with the phase transition. Optical evidence for strain relaxation and multiphase coexistence is observed through the transition from 150 to 165 K. The multiphase coexistence is seen as the formation of FMM "nanoneedles" with widths less than 100 nm and lengths of at least several micrometers at temperatures well below $T_C$. The work demonstrates polarized NSOM as a technique for the study of first-order solid-state phase transformations on the nanometer spatial scale.**

Optical microscopy has long been employed to investigate many aspects of the microstructures of metals.[1] Included in these aspects is the strain-induced formation of martensitic steel where strain is detected by polarized microscopy.[2] Recently, it has been suggested that ferromagnetic metal (FMM) to charge-ordered insulator (COI) phase transition in the manganites are martensitic in nature,[3] and accordingly optical microscopy has been used to characterize the transitions. Transmission electron microscopy (TEM) is a high-resolution imaging tool that also has been brought to bear both on metals and the manganites, but strain effects are difficult to observe in TEM. Near-field scanning optical microscopy (NSOM) possesses strengths of both techniques, high resolution and the ability to image microstructure. As lattice mismatches become larger and strain results in smaller twins, the high resolution becomes critical to image twins and strain effects on the submicrometer level. NSOM has the further advantage of also providing topographic data simultaneously. However, NSOM comes with its own particular challenges such as polarization control, image interpretation, low-temperature operation, and slow scan rates.

In this paper, we report on the near-field optical imaging of the electronic phases of $Nd_{1/2}Sr_{1/2}MnO_3$. To the best of our knowledge, this is the first report on solid-state phase transitions using near-field optical techniques.

The competing thermodynamic phases for $Nd_{1/2}Sr_{1/2}MnO_3$ are a low temperature, CE-type COI that is accompanied by spin order and $e_g$ orbital ordering, a FMM with a transition temperature of about 160 K, and a paramagnetic insulator (PM) with a transition temperature of about 250 K.[4] The equilibrium phase at a particular temperature depends on the competition of the microscopic processes occurring on the manganese ions including the Jahn−Teller effect, double exchange, and on-site Coulomb repulsion. Because the interesting phase transitions occur in the solid state and generally involve the lattice degrees of freedom, they are usually accompanied by inhomogeneous strain and twinning. The transition from the COI phase to the FMM phase is first-order and involves a change in crystal structure. The first-order nature results in discontinuous and hysteretic changes in resistivity,[5] reflectance,[6] magnetic susceptibility,[6] and lattice constant. At room temperature, the crystal structure of $Nd_{1-x}Sr_xMnO_3$ is orthorhombic but can be understood as a distorted cubic perovskite crystal. The octahedra formed by Mn atoms surrounded by six O atoms is apically compressed and tilted relative to the crystallographic axes. The distortions result in a pseudocubic lattice and differences of Mn−O bond lengths along the *c*-axis and within the *ab* plane that increases from about 0.5% in the FMM and PM phases to about 1.1% in the COI phase for $Nd_{1/2}Sr_{1/2}MnO_3$.[4] There are also differences in these bond lengths within the *ab* plane. As a result, the optical response for light polarized along each of the orthogonal crystal axes can be different.

* Corresponding author. E-mail: pkolb@lps.umd.edu.
† Laboratory for Physical Sciences, University of Maryland.
‡ Department of Physics, University of Maryland, College Park, MD 20742.
§ Physical and Materials Chemistry Division, National Chemical Laboratory, Pune 411008, India.
⊥ Department of Physics, University of Tsukuba, Tsukuba 305-8571 Japan.

10.1021/nl0629761 CCC: $37.00 
**Published on Web 05/15/2007**

This optical anisotropy can be exploited to observe "optical" domains of differing axis orientation within each electronic phase. While far-field imaging of large-scale optical domains can be found elsewhere,[6] the focus of this paper is the evolution of contrast in near-field images of anisotropy in twins with temperature near $T_C$. Such images display a narrow needle-like feature along the twin boundary which is interpreted as a forming FMM "nanoneedle."

The $Nd_{1/2}Sr_{1/2}MnO_3$ sample studied in this work is single crystal grown by the floating zone method.[7] The sample was polished with a 9.8 pH, 0.05 $\mu$m silica suspension. The resulting surface was shown to be locally smooth but faceted, as seen by atomic force microscopy (AFM). The faceting is likely due to differential polishing rates along different crystal axes. Following the recipe of H. J. Lee et al., the sample was also annealed in an $O_2$ atmosphere at 1000 °C to remove surface damage.[8] The resulting surface was locally smoother but also demonstrated a higher density and complexity of faceting. The latter may be due to passage in to and out of a rhomohedral phase during annealing. The existence of this additional phase is suggested by the phase diagram of the similar manganite $La_{1-x}Ca_xMnO_3$.[9] Some of the topography from the polishing/annealing process is "frozen-in" in the sense that it persists even as the surface undergoes upheaval during the FMM−COI phase transitions. These frozen-in features sometimes appear in far-field micrographs[6] and near-field images and are not associated with optical domains. Far-field imaging shows COI−FMM phase coexistence from about 155 to 168 K.[6]

The near-field images are generated in the so-called emission mode where light is sent through the tip and collected in the far-field. The resolution of the NSOM images is roughly 100 nm, the size of the probe aperture. The near-field probes were fabricated by the common technique of pulling a laser-heated fiber and coating the tapered region with aluminum.[10] The polarization at the aperture is controlled by means of a standard three-paddle polarization manipulator. These paddles stress the fiber as they are mechanically rotated and act to rotate the polarization state. In principle, the paddles can transform any input state to any output state. Because the paddles, fiber bends, and tip act together as a single arbitrary rotator, orthogonal input states map into orthogonal output states. This can be realized by launching orthogonal, linearly polarized beams into the NSOM fiber. By trial and error, linear polarization of the far-field emissions of tips could be achieved with a typical extinction ratio of 200:1. In the experiment, the emitted light interacts with the sample in the near-field and is collected in the far-field by means of a lens and a parabolic mirror. The collection optics and method of polarization control are illustrated in Figure 1.

With the tip in near-field approach to the sample, it was not possible to determine the output polarization state. Instead the tip was prescanned over a region with optical anisotropy, while the paddles were adjusted to maximize contrast. Typically, the orthogonal polarization state was also used to scan the sample. The overall or average light signal collected varied from scan to scan by as much as a factor of

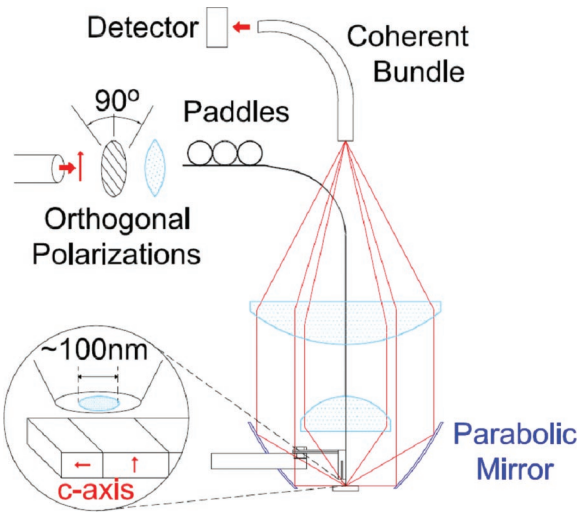


**Figure 1.** Collection optics and polarization control.

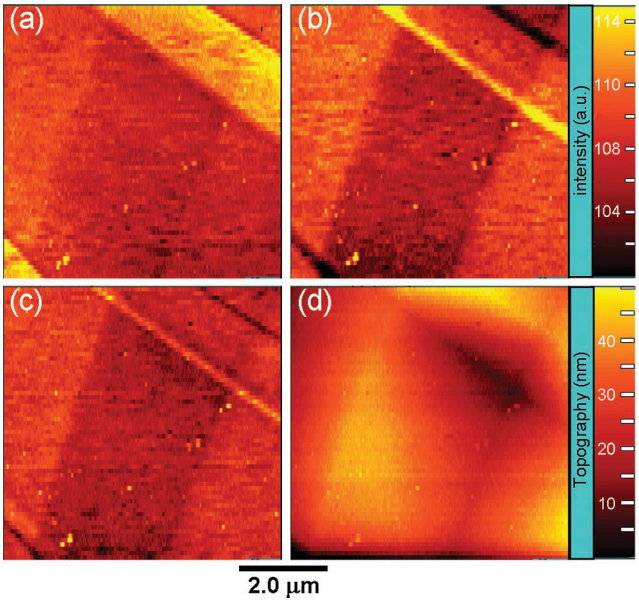


**Figure 2.** NSOM scans of the COI phase using 633 nm light. Polarization is adjusted to maximize contrast in (a), the orthogonal polarization is used in the (b), and an arbitrary polarization in (c). The topography is shown in (d). The temperature is 77 K.

2. The sample reflectance, the NSOM probe throughput, and the light detection system can all exhibit polarization sensitivity and contribute to this variation. For convenience of viewing, each NSOM image is rescaled so that the lowest value is 100.

Generally speaking, NSOM scans of the sample in the COI, FMM, and PM phases show common characteristics. Typical scans are shown in Figures 2, 3, and 4. Topographic images, generated simultaneously with the NSOM light intensity images, reveal a faceted surface. These facets are typically observable in the NSOM images and fall into one of two types. The first type of facet exhibits weak contrast, on the order of 2%. The contrast of these facets is virtually independent of polarization. Conversely, contrast of the second type of facet can be as strong as 10% depending on the polarization used to view them. Typically, the contrast of these facets can even be reversed when viewed with

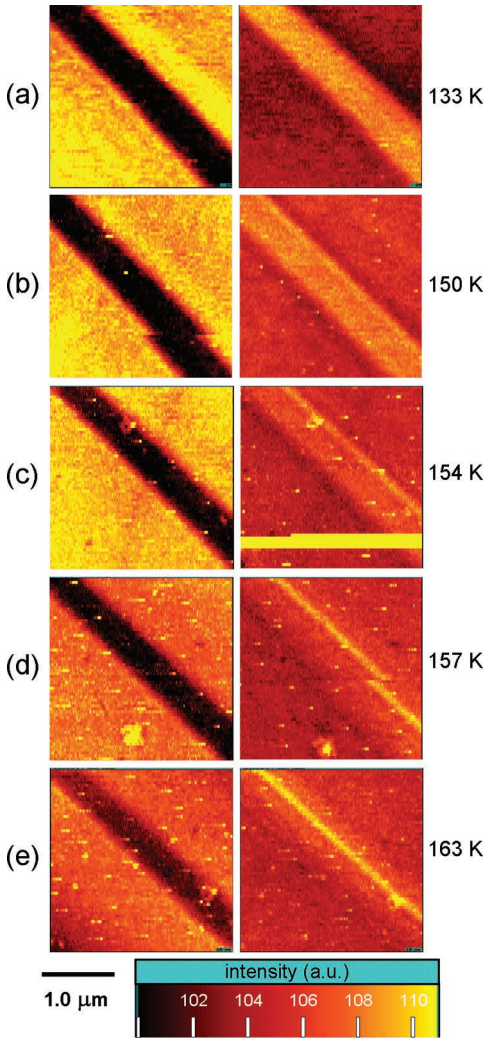


**Figure 3.** NSOM scans of the COI phase as temperature is swept upward. Orthogonal polarizations are used in left and right scans. The wavelength used is 633 nm.

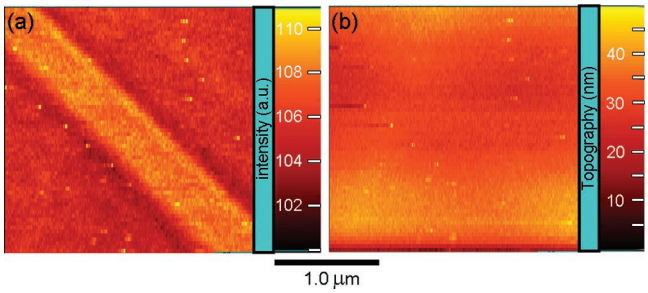


**Figure 4.** NSOM scan (a) and associated topography of the COI twin (b) at 150 K. Compared to Figure 2, there is very little topography associated with the twin.

orthogonal polarizations. These facets frequently exhibit narrow features on their edges with polarization dependent contrast.

Far-field and near-field images are complementary, each aiding the interpretation of the other. Although far-field resolution is significantly less, large areas can be imaged quickly. Used in concert with the near-field, a more complete picture emerges. For instance, faceting of the surface suggested by far-field images is confirmed in the near-field. As in the near-field, some faceted regions with different crystal axis orientations exhibit different polarization contrast due to optical anisotropy. Far-field imaging shows these regions, called variants, can be hundreds of micrometers wide with twins of micrometer scale width. Near-field imaging, on the other hand, is best suited for imaging of twins only. These twins can exhibit polarization effects near their edges,[6] which are less commonly seen in the far-field. This is probably because, due to their small widths, edge effects seen in the near-field would be difficult to observe and impossible to resolve in the far-field. Also seen in the far-field, twins appear to have faceted regions running through them that exhibit little or no polarization contrast. As mentioned, these regions probably emerged as part of the topography that is frozen-in during the polishing/annealing process and are not associated with different crystal axis orientations. Dramatic edge effects are not seen in these types of facets. Because edge effects are occasionally seen in the far-field[6] and because they are seen in the near-field only coincident with optical domain topography, they are probably not artifacts. A likely cause of these anisotropic edge effects is strain near the twin boundaries.

Differences in contrast between the near-field and far-field are primarily due to a difference in the effective angle of illumination. The NSOM probe and sample can be modeled as a waveguide in which rays at large angles to the normal are most efficiently emitted and detected.[11] Conversely, far-field illumination and collection is essentially a cone centered on the normal. As a result, contrast of COI optical domains in the near-field is significantly less than in the far-field.

With the general features common to NSOM scans now discussed, we now focus on the specifics of the NSOM scans. Figure 2 shows a near-field scan of the COI phase. This figure shows the presence of frozen-in facets in near-field intensity and topographic scans. These facet boundaries run parallel in the scans at about 65° counterclockwise from the *x*-axis. From scan to scan, the near-field intensity signal from these facets is only weakly polarization dependent. Contrast from these regions presumably comes from a preference in the illumination/detection system. Running through the frozen-in facet boundaries are faceted stripes that make an angle of about 35° clockwise from the *x*-axis. These stripes exhibit a stronger polarization contrast, including contrast reversal and edge effects, and are taken to be the signature of optically anisotropic twin domains. Another indication that the edge effects are not artifacts comes from Figure 2b, where a bright (dark) edge corresponds to a facet valley (ridge). Because of the sample effectively acting like a lens when forming the NSOM image, a sample valley (ridge) would be expected to artificially decrease (increase) the NSOM signal.[12]

Perhaps the most interesting features of the NSOM scans of Figure 2 are the alternating bright and dark edges of the twin boundaries. As previously mentioned, a likely cause of the anisotropic edge effects is strain. In this picture, stress causes the Mn−O bonds to change length and thus introduces additional optical anisotropy. Because the edges alternate between bright and dark, the stress should also alternate from

tensile, perpendicular to one side of the boundary, to compressive, perpendicular to the other side. Local strain conditions would be expected to vary, and accordingly, edge effects are not present in every NSOM scan. Not surprisingly, there is a rather noticeable topography associated with the twin.

Figure 3 shows the near-field intensity scans from a typical temperature sweep where a COI twin stripe is observed and followed as a function of temperature. This stripe appears dark for one polarization and bright in the orthogonal polarization. As temperature is increased, the exact spot along the stripe changes from scan to scan, but common artifacts from particles can sometimes be seen. As the temperature is swept upward, there are gradual changes in the overall polarization-dependent contrast of the twin. Additionally, a bright needle appears on the upper boundary of the twin for one polarization. These needles are micrometers long, and their width must be the width of the tip, 100 nm or less. Because of the discontinuous first-order nature of the COI to FMM transition, attempts to observe the growth of the needle beyond 163 K were unsuccessful. During two attempted scans at 167 K, the approach feedback controlling the tip-to-sample height began to jump discontinuously, presumably because the sample surface was heaving during the COI to FMM phase transition, causing the NSOM tip to suddenly change height. After some time, order was restored. Further scans (not shown) at 167 K began to be stable again, but due to the phase transition, the NSOM images no longer resembled those of lower temperature, and the needle could no longer be identified.

Unlike the bright and dark edge effects in Figure 2, the bright edge in Figure 3 is probably not directly associated with strain. If this were to be the case, the strain would have to evolve with temperature only within a range fortuitously close to $T_C$. Additionally, one might expect a significant change in topography which is not observed. In fact, the associated topography, as shown in Figure 4, is rather minimal, and no changes are detected.

Interpreting the emergence of the bright edge in terms of the COI to FMM phase transition is much more consistent with the results of far-field imaging. In this interpretation, a bright FMM needle nucleates along the top twin boundary and brightens as the temperature approaches $T_C$, while the contrast of the COI twin-stripe gradually fades due to a temperature dependence of the reflectance, differences in polarization, a thermal/mechanical light collection artifact, or a combination of these factors.[13] As seen in the far-field, FMM phase domains appear to nucleate along COI variant boundaries at temperatures as low as 155 K, grow slowly at first as temperature increases, and merge with other domains.[6] Less frequently and at temperatures around 165 K much closer to $T_C$, sharp FMM wedges can be seen to form along COI twin boundaries. An idealized schematic of this wedge formation is shown in Figure 5. However, in these far-field images, the FMM needles appear dark, not bright as they do in the near-field. Unlike in the far-field, the FMM and COI phase domains have roughly the same brightness in the near-field and thus are more difficult to distinguish. In both

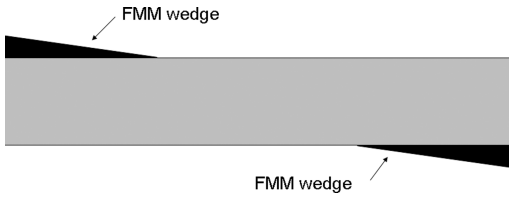


**Figure 5.** Illustration of FMM wedge formation along COI twin boundaries. Far-field imaging shows these wedges to be several tens of micrometers in length.

the COI phase and FMM phase, the near-field intensity is strongly polarization dependent and can vary roughly by a factor of 2 from minimum to maximum. Even though the brightness of each NSOM scan has been rescaled for ease of viewing and to adjust for intensity drifts, the average brightness of each scan is different. In the case of Figure 3, the right images are about 1.5 times dimmer than the left images. Thus, it is reasonable that forming FMM phase domains would appear bright in the right images where the COI phase is dim. Consistent with far-field imaging, the FMM phase can and does form at COI twin boundaries. However, the higher spatial resolution of NSOM shows that on the nanoscale FMM nucleation on COI twins starts as low as 150 K.

Though the apparent width of the needle is roughly equal to that of the width of the NSOM probe aperture of approximately 100 nm for all measured temperatures, the growing brightness with increasing temperature implies that the illuminated FMM area under the tip is also increasing. Therefore, for temperatures up to 163 K, the actual needle width increases but never exceeds the aperture diameter. Presumably, the width would continue to grow with temperature had it been permitted to do so. However, by the time 167 K is reached, the scanned region has most likely wholly transitioned to the FMM phase, possibly being overwhelmed by a FMM domain originating elsewhere in the sample. In addition to the initial NSOM feedback instability at 167 K and the wholesale changes of the NSOM images already mentioned, far-field imaging and the temperature dependence of the magnetic susceptibility indicate that, by 167 K, the transition to the FMM phase is mostly complete. Although far-field imaging shows phase coexistence from about 155 to 170 K, the temperature range where the areas of COI and FMM domains are comparable in size is only about 1 K. To illustrate this, the ratio of FMM area to image area is plotted verses temperature for a particular far-field image area of about 0.28 $mm^2$ along with the normalized magnetic susceptibility in Figure 6. The presence of the FMM phase as observed in the near-field helps account for the nonzero magnetization at temperatures substantially lower than $T_C$.

In summary, optical anisotropy in twins, strain effects, and multiphase coexistence in $Nd_{1/2}Sr_{1/2}MnO_3$ have successfully been imaged using polarized NSOM. A detailed study of far-field imaging is critical to the proper interpretation of the near-field images. Taken in conjunction, the two sets of images lead to a consistent description. In both near-field and far-field imaging, optical anisotropy is observed in the

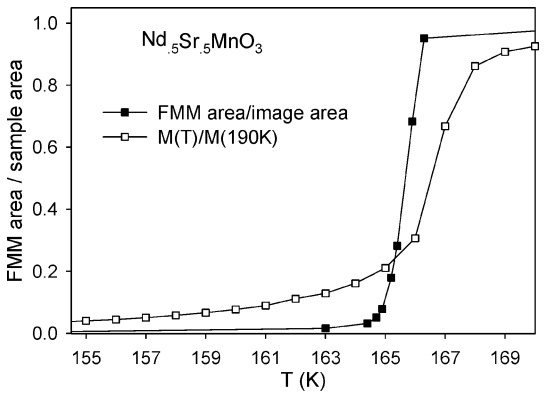


**Figure 6.** The ratio of far-field observed area of FMM domains to the total observed area and the normalized magnetic susceptibility of the sample vs temperature.

low-temperature COI phase, the ferromagnetic metal FMM phase, and the PM phase. The anisotropy is attributed to differences in Mn−O bond lengths in different crystallographic orientations. NSOM images show that optical domains consistent with twinning have an associated topography. Consistent with far-field imaging, polarization-dependent features are observed in the near-field on twin boundaries and are attributed to tensile or compressive strain. In the near-field, "nanoneedles" are observed to form and grow in strength on COI twin boundaries as the temperature approachs the transition temperature. Consistent with far-field imaging, these bright regions are interpreted to be FMM needles that form at points where the tensile strength is large. However, the higher spatial resolution of NSOM reveals FMM nucleation on COI twin boundaries well below $T_C$, at temperatures where far-field imaging is only able to show FMM nucleation on COI variant boundaries. Overall, the work demonstrates the use of polarized NSOM as a technique for the study of first-order solid-state phase transformations. NSOM's achievable spatial scale of several tens of nanometers makes it ideal for observing the onset and development of multiphase coexistence as phase transitions are approached.

**Acknowledgment.** This work was supported by the NSF-MRSEC program of the NSF grant no. DMR-00-80008.

## References

(1) Avinoam Tomer, *Structure of Metals Through Optical Microscopy*; ASM International: Materials Park, OH, 1991.

(2) Nishiyama, Z. *Martensitic Transformation*; Fine, M., Meshii, M., Wayman, C., Eds.; Academic Press: New York: 1978; pp 23.

(3) Podzorov, V.; Kim, B. G.; Kiryukhin, V.; Gershenson, M. E.; Cheong, S.-W. *Phys. Rev. B* **2001**, *64*, 140406.

(4) Kajimoto, R.; Yoshizawa, H.; Kawano, H.; Kuwahara, H.; Tokura, Y.; Ohoyama, K.; Ohashi, M. *Phys. Rev. B* **1999**, *60*, 9506.

(5) Jung, J. H; Lee, H. J.; Noh, T. W.; Choi, E. J.; Moritomo, Y.; Wang, Y. J.; Wei, X. *Phys. Rev. B* **2000**, *62*, 481.

(6) Kolb, P. W.; Romero, D. B.; Drew, H. D.; Moritomo, Y.; Souchkov, A. B.; Ogale, S. B. *Phys. Rev. B* **2004**, *70*, 224415.

(7) Moritomo, Y.; Kuwahara, H.; Tomioka, Y.; Tokura, Y. *Phys. Rev. B* **1997**, *55*, 7549.

(8) Lee, H. J.; Jung, J. H.; Lee, Y. S.; Ahn, J. S.; Noh, T. W.; Kim, K. H.; Cheong, S.-W. *Phys. Rev. B* **1999**, *60*, 5251.

(9) Schiffer, P.; Ramirez, A. P.; Bao, W.; Cheong, S.-W. *Phys. Rev. Lett.* **1995**, *75*, 3336.

(10) Valaskovic, G. A.; Holton, M.; Morrison, G. H. *Appl. Opt.* **1995**, *34*, 1215.

(11) A model of NSOM contrast treats the NSOM probe as a shadowed point source. Rays at larger angles to the normal transmit into the far-field with less loss because they experience fewer reflections between the metalized tip and sample. Accordingly, *s* and *p* modes have different reflectivities and transmit with different efficiencies. Alternatively, the metalized tip in close proximity to the sample can be thought of as an effective waveguide. Depending on the properties of the sample, the waveguide transmission can be sensitive to $E_x$ or $E_z$, which is present in the near-field. Boundary conditions require continuity of the tangential electric field. As a result, all modes from $E_x$ are cut off when the tip−sample spacing goes below $\lambda/2$ for a metal sample. Because this constraint is more severe for metal samples, their response to $E_x$ is reduced more than it is for insulators. Conversely, the condition of tangential continuity does not apply to $E_z$. Surface currents act to support the tangential **H** field. Higher conductivity allows metals to transmit this mode more effectively than insulators.

(12) Durkan, C.; Shvets, I. V. *J. Appl. Opt.* **1998**, *83*), 1171.

(13) In principle, the differences in bond lengths within the *ab* plane that give rise to optical anisotropy are temperature dependant. Additionally, the polarization used from scan to scan may not be the same because it was necessary to adjust the polarization with temperature to compensate for the temperature-dependant polarization rotation of fiber bends in the cryostat. Furthermore, the collection efficiency for a particular polarization was likely changing as a function of temperature. In general, the far-field collection efficiency of NSOM systems is dependant of the geometry of the collection system. In principle, the lens and parabolic mirror used in these experiments provides symmetric collection with no polarization sensitivity. In reality, the system demonstrates significant polarization sensitivity due to differences in focus, alignment, and orientation of the optical axes with the sample and asymmetric blocking of light in the optical path by the *z*-approach mechanism. In an alternative interpretation of the fading contrast, the FMM and COI phases mix uniformly and gradually with temperature. However, this picture is inconsistent with the results of the far-field imaging where regions of different phase are well demarcated.

NL0629761